JACS
JOURNAL OF THE AMERICAN CHEMICAL SOCIETY

COMMUNICATION

pubs.acs.org/JACS

# Compositionally Tunable $Cu_2ZnSn(S_{1-x}Se_x)_4$ Nanocrystals: Probing the Effect of Se-Inclusion in Mixed Chalcogenide Thin Films

Shannon C. Riha,[†,§] B. A. Parkinson,[*,‡] and Amy L. Prieto[*,§]

[‡]Department of Chemistry and School of Energy Resources, University of Wyoming, Laramie, Wyoming 82071, United States
[§]Department of Chemistry, Colorado State University, Fort Collins, Colorado 80523, United States

Supporting Information

**ABSTRACT:** Nanocrystals of multicomponent chalcogenides, such as $Cu_2ZnSnS_4$ (CZTS), are potential building blocks for low-cost thin-film photovoltaics (PVs). CZTS PV devices with modest efficiencies have been realized through postdeposition annealing at high temperatures in Se vapor. However, little is known about the precise role of Se in the CZTS system. We report the direct solution-phase synthesis and characterization of $Cu_2ZnSn(S_{1-x}Se_x)_4$ nanocrystals ($0 \le x \le 1$) with the aim of probing the role of Se incorporation into CZTS. Our results indicate that increasing the amount of Se increases the lattice parameters, slightly decreases the band gap, and most importantly increases the electrical conductivity of the nanocrystals without a need for annealing.

Multicomponent chalcogenide nanocrystals (MCNs) are capable of revolutionizing the manufacture of thin-film solar cells.[1−7] They offer the advantage of simple, low-temperature deposition, which can lead to inexpensive large-scale production. Furthermore, MCNs offer the additional advantage of having tunable structural, optical, electronic, and defect properties that all can influence photovoltaic (PV) properties.[1,8−10] For example, it is known that in the $Cu(In,Ga)Se_2$ system, optimizing the In:Ga ratio changes the band gap to maximize solar cell efficiencies. Mixed chalcogenides also allow band gap tunability, offering an alternative to the quantum-confinement effect, as this effect is generally lost when nanocrystals are annealed into dense films.[2,11]

$Cu_2ZnSnS_4$ (CZTS) is receiving increased attention for use in low-cost thin-film PVs[3,6,12,13] because of its earth-abundant constituents, optimal band gap, and high absorption coefficient. CZTS crystallizes in the chalcopyrite crystal system with Cu and Zn cations sharing one Wyckoff position.[14,15] Theoretical and experimental work has shown that the electronic properties can be tuned by varying the Cu:Zn ratio as well as their ordering.[12,14−16] In both bulk and nanocrystal thin-film PV devices, Cu:(Zn + Sn) = 0.8 and Zn:Sn = 1.2 ratios lead to the highest reported power conversion efficiencies.[3,12,16,17] Furthermore, Chen et al.[8] calculated that the band gap of CZTS,Se solid solutions can be controlled by varying the S:Se concentration. They predicted that the band gap linearly decreases with increasing Se content. Herein we report the first direct solution-phase synthesis of $Cu_2ZnSn(S_{1-x}Se_x)_4$ nanocrystals with control over $x$ from 0 to 1, where the measured band gaps across the solid-solution range are consistent with theoretical predictions.

Despite the similarities between bulk and nanocrystal thin films, PV devices prepared from CZTS nanocrystals without postdeposition annealing at high temperatures ($\ge$500 °C) are <1% efficient.[6,18] Following the procedures from the CIGS literature, Guo et al.[3] recently reported that annealing CZTS nanocrystals in the presence of Se vapor at 500 °C resulted in a PV device with 7.2% conversion efficiency. However, the final composition of the annealed films could not be tuned because high-temperature annealing steps provide little control over the S:Se ratio. The large efficiency increase is surprising if the incorporation of Se simply tunes the band gap. Two hypotheses in the literature suggest that the inclusion of Se (i) creates $Cu_2ZnSn(S_{1-x}Se_x)_4$ alloys that alter the optical and electronic properties of the films or (ii) facilitates enhanced grain growth.[2] A third possible but related hypothesis is that the grain boundaries are passivated by Se-rich surfaces, resulting in a lower band gap surface layer, hence removing potential barriers for grain-to-grain carrier transport. A first step in testing these hypotheses is the development of a robust synthesis for phase-pure, compositionally controlled $Cu_2ZnSn(S_{1-x}Se_x)_4$ (CZTS,Se) nanocrystals.

The synthesis of CZTS,Se nanocrystals was carried out using a hot-injection method adapted from a previous report.[13] Briefly, copper(II) acetylacetonate, zinc acetate, and tin(IV) acetate were combined in appropriate ratios [Cu:(Zn + Sn) = 0.8 and Zn:Sn = 1.2] under inert conditions with oleylamine (OLA). The flask was heated under vacuum to 150 °C and then cooled to 125 °C after 5 min, where it was held until injection. Meanwhile, elemental S and Se were mixed with OLA and $NaBH_4$ via sonication. Trioctylphosphine oxide (TOPO) was heated in a separate flask to 325 °C, at which point both the metal and chalcogenide precursors were simultaneously injected. The growth temperature was then reduced to 285 °C, and the reaction was quenched after 5 min. Full experimental details can be found in the Supporting Information (SI).

Control of the stoichiometry of MCNs is challenging, especially when five elements are involved in the reaction. Therefore, balancing the relative precursor reactivities is key to producing the desired composition without unwanted side products.[9,10] Compositionally controlled CZTS,Se nanocrystals were obtained only when elemental S and Se were sonicated together with $NaBH_4$ and OLA to balance the reactivities of S and Se. It was recently reported that $NaBH_4$ in the presence of hydrophobic alkylamines (e.g., OLA) can reduce Se powder to form alkylammonium selenide complexes.[19] We explored keeping the OLA−Se

**Received:** June 23, 2011
**Published:** September 01, 2011





dx.doi.org/10.1021/ja2058692 | J. Am. Chem. Soc. 2011, 133, 15272–15275

**Table 1. Compositional Analysis, Lattice Parameters ($a$ and $c$), and Band Gap Energies of $Cu_2ZnSn(S_{1-x}Se_x)_4$ Nanocrystals**

| calcd composition | Cu:Zn:Sn:S:Se precursor ratio | Cu:Zn:Sn:S:Se ratio determined by EDS | $a$ (Å) | $c$ (Å) | $E_g$ (eV) |
|---|---|---|---|---|---|
| $Cu_2ZnSnS_4$ ($x = 0$) | 1.8:1.2:1:7:0 | 1.9(2):1.1(3):1.0(1):4.1(4) | 5.41 | 10.81 | 1.54(1) |
| $Cu_2ZnSn(S_{0.9}Se_{0.1})_4$ ($x = 0.1$) | 1.8:1.2:1:6.3:0.7 | 2.0(2):1.1(3):1.0(1):3.5(2):0.4(1) | 5.44 | 10.89 | 1.52(2) |
| $Cu_2ZnSn(S_{0.5}Se_{0.5})_4$ ($x = 0.5$) | 1.8:1.2:1:3.5:3.5 | 2.0(2):1.1(1):1.0(1):2.1(2):1.8(2) | 5.48 | 10.95 | 1.50(2) |
| $Cu_2ZnSn(S_{0.1}Se_{0.9})_4$ ($x = 0.9$) | 1.8:1.2:1:0.7:6.3 | 1.8(2):1.2(2):1.0(1):0.3(1):3.7(1) | 5.60 | 11.17 | 1.48(1) |
| $Cu_2ZnSnSe_4$ ($x = 1$) | 1.8:1.2:1:0:7 | 1.9(2):1.1(1):1.0(1):4.0(2) | 5.61 | 11.28 | 1.47(2) |

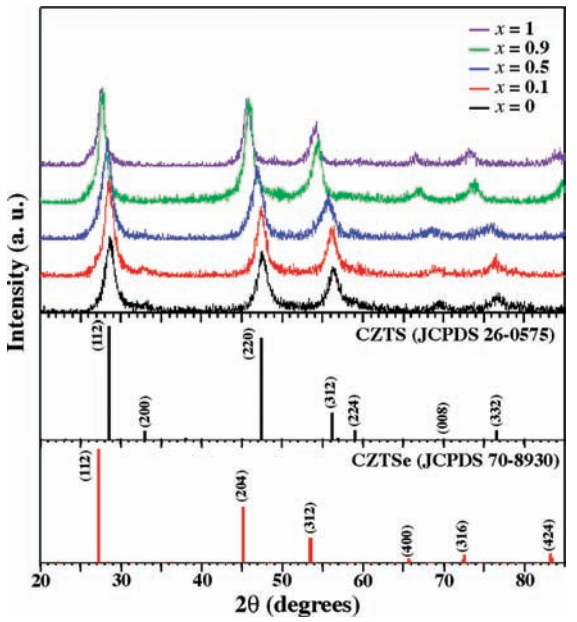


**Figure 1.** XRD patterns of $Cu_2ZnSn(S_{1-x}Se_x)_4$ nanocrystals for various values of $x$. The standard XRD patterns for CZTS and CZTSe are shown below.

and OLA−S precursors separate (vs mixing them in one vial) prior to injection. Keeping the S and Se precursors separate often resulted in a Se-rich composition or in phase separation of CZTS and CZTSe nanocrystals. We speculate that this could be due to variations in the relative chalcogenide speciation, and thus the reactivity, at the time of nucleation. Nucleation occurs immediately upon injection; therefore, if the OLA−Se/OLA−S mixture contains multiple species, preferential incorporation of Se or distinct phase nucleation could give the observed results. Hence, a homogeneous mixture of OLA−S and OLA−Se was required for the preparation of compositionally controlled CZTS,Se nanocrystals. Once the reactivities of S and Se were controlled, the metal: chalcogen ratios and temperature were optimized to prepare the desired S:Se ratios and inhibit the formation of unwanted side products.

The compositions of the CZTS,Se nanocrystals were determined using energy-dispersive X-ray spectroscopy (EDS) and are listed in Table 1. The ratios of the S and Se precursors and the obtained S:Se ratios in the final CZTS,Se nanocrystals are in close agreement. This indicates that the reactivities of the chalcogen precursors were balanced.

Figure 1 shows powder X-ray diffraction (XRD) data for CZTS,Se nanocrystals synthesized with $x = 0-1$. The nanocrystal sizes for each composition were determined by the Williamson−Hall method and are found in Table S1 in the SI. The XRD data indicate the incorporation of Se in the CZTS nanocrystals. At $x = 0$, the diffraction peaks can be indexed to those of kesterite $Cu_2ZnSnS_4$ (JCPDS no. 26-0575). As the Se content increases, the larger Se atoms (1.98 Å) replace the smaller S atoms (1.84 Å), resulting in an increase in the lattice parameters, as shown by the shift in the diffraction peaks to lower values of $2\theta$ (Figure S1a in the SI). Furthermore, at $x = 0$, the small peak at $2\theta = 32.99°$ can be indexed to the (200) plane of CZTS. As the S:Se ratio decreases, this peak intensity decreases, and the peak disappears for $x \geq 0.9$. Similarly the diffraction peak at $2\theta = 83.18°$, corresponding to the (424) plane of CZTSe, appears for $x \geq 0.9$. At $x = 1$, the diffraction pattern corresponds to $Cu_2ZnSnSe_4$ (JCPDS no. 70-8930). The $Cu_2ZnSn(S_{1-x}Se_x)_4$ lattice parameters $a$ and $c$ (Table 1) were calculated as a function of $x$ from the XRD data and found to vary linearly with Se content, as expected on the basis of Vegard's Law (Figure S1b,c).

Figure 2a−e displays high-resolution transmission electron microscopy (HRTEM) images highlighting the lattice fringes of individual $Cu_2ZnSn(S_{1-x}Se_x)_4$ nanocrystals representative of the various compositions. Lattice spacings were calculated by averaging measurements from multiple fringes on each particle and from multiple particles. At $x = 0$, the measured lattice spacing was 3.10 ± 0.04 Å, corresponding to the $Cu_2ZnSnS_4$ (112) crystal plane. As the value of $x$ increased from 0 to 1, the lattice spacing increased. For $x = 1$, the measured $d_{(112)}$ spacing was 3.27 ± 0.04 Å. Again, Vegard's Law was obeyed when the $d_{(112)}$ spacing was plotted as a function of $x$ (Figure 2f). TEM images of the CZTS,Se nanocrystals with $x$ ranging from 0 to 1 (Figure S2) showed average particle sizes ranging from 7.8 nm when $x = 0$ to 11.0 nm when $x = 1$, which are consistent with those calculated from line broadening of the diffraction peaks (a statistical analysis of the particle sizes can be found in Table S1).

The synthesis of pure $Cu_2ZnSn(S_{1-x}Se_x)_4$ MCNs with varying S:Se ratios is a direct route for examining the hypotheses regarding annealing of CZTS nanocrystals in Se vapor.[3,16] To test the first hypothesis (suggesting that CZTS,Se alloys alter the optical properties), UV−vis spectroscopy was used to determine the band gap of each CZTS,Se alloy synthesized. The band gap energies ($E_g$) were calculated by plotting the square of $\alpha h\nu$ [where $\alpha$ is the absorption coefficient obtained from the UV−vis spectra of solutions of CZTS,Se nanocrystals (Figure S3a), and $h\nu$ is the photon energy] as a function of $h\nu$ and extrapolating the linear portion to the $x$ intercept (Figure S3b). Figure 3 shows a plot of $E_g$ as a function of composition. The $E_g$ values determined from the optical absorption of the CZTS,Se colloidal nanocrystals (Table 1) range from 1.54 eV for $x = 0$ to 1.47 eV for $x = 1$, which are comparable to experimental bulk values reported for CZTS and CZTSe, respectively.[5,8,13] Increasing the Se concentration reduces $E_g$, although a tunability window of ~70 meV is not likely to drastically increase the PV properties in a single-junction device, as observed by Guo et al.[3] Therefore, the first hypothesis is not a

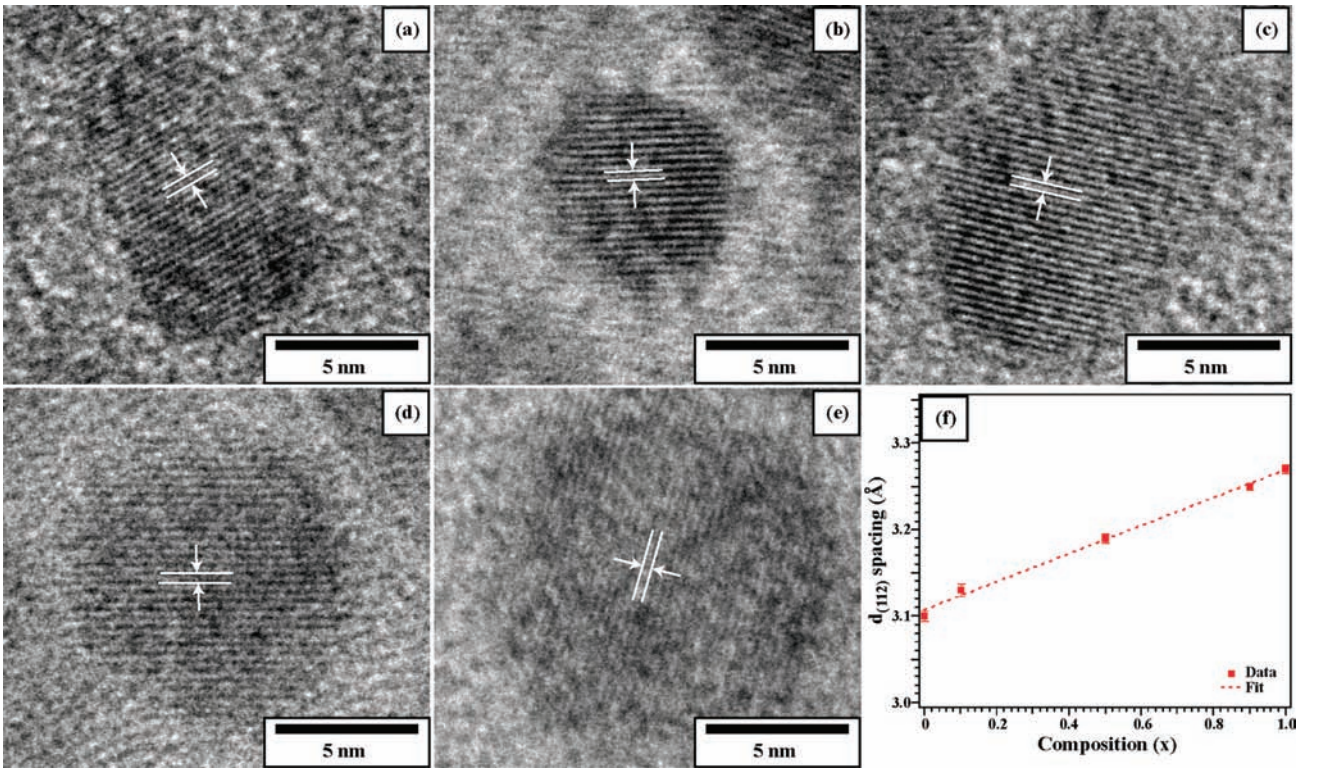


**Figure 2.** (a–e) HRTEM images of the $d_{(112)}$ lattice fringes for $Cu_2ZnSn(S_{1-x}Se_x)_4$ nanocrystals with $x$ = (a) 0, (b) 0.1, (c) 0.5, (d) 0.9, and (e) 1. (f) Plot of the lattice spacing vs $x$, which follows Vegard's Law.

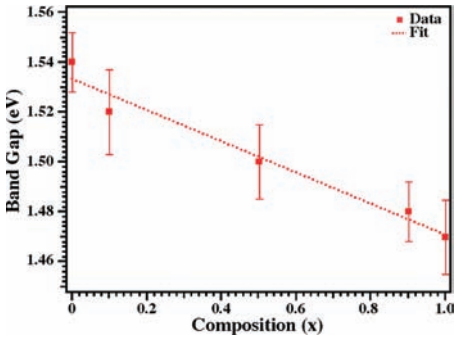


**Figure 3.** Band gap energies determined from the optical absorption of $Cu_2ZnSn(S_{1-x}Se_x)_4$ colloidal nanocrystals. A linear decrease was observed with an increase in Se content.

reasonable explanation for the role of Se in improving the efficiency of thin-film CZTS,Se devices.

The preliminary results discussed herein suggest that the second hypothesis may help to explain the role of Se in CZTS nanocrystal thin films. On the basis of literature results for $Cu(In_{1-x}Ga_x)S_2$-based solar cells, thermodynamic calculations indicate that the S atoms are replaced by Se when the films are annealed at high temperatures with an elevated partial pressure of Se.[2] The authors stated that the replacement of the S atoms by the larger Se atoms increases the crystal lattice parameters, causing the films to expand and leading to improved grain growth. In support of this claim, when Guo et al. annealed their CIGS nanocrystal thin films in a S-only vapor, they did not observe grain growth, suggesting that Se is responsible for forming densely packed grains in that material.[2] The inclusion of Se in our CZTS nanocrystals also increased the lattice parameters, as determined by XRD; however, this would only result in a very minimal increase in grain size. Rather significant grain growth requires surface diffusion or other mechanisms of mass transport.

A more likely explanation is that in this system Se is a better vapor-transport agent than S, which would have a more dramatic effect on grain growth than simply an increase in lattice parameters. To provide additional evidence supporting this hypothesis, the CZTS,Se thin films made from the syntheses reported in this manuscript were annealed, but at a much lower temperature (350 °C) than that reported by Guo et al.[3] and Todorov et al.[16] We observed a dramatic difference because pure CZTS nanocrystal films did not transport during annealing, whereas in the case of some Se-rich CZTS,Se films, material was transported completely off the substrate into the quartz tube. Therefore, these preliminary results support the second hypothesis that introducing Se into CZTS does enhance grain growth because Se provides a better mechanism of mass transport than S does.

The results from Guo indicate that the grain boundaries present in CZTS nanocrystal thin films are the main cause of the observed low efficiencies for these films without a postdeposition annealing treatment.[3] Therefore, reducing the number of grain boundaries should enhance electron transport and result in an increase in device efficiency. An alternative hypothesis, hypothesis (iii), is that the grain boundaries are passivated by a lower-band-gap Se-rich surface, reducing the potential barriers for grain-to-grain charge transport. As a way to begin to probe this hypothesis, we examined the effects of Se on the electrical conductivity of nonannealed nanocrystal CZTS,Se powders. Figure S4 shows the composition dependence of the conductivity,

which increases as a function of Se concentration. Despite the small change in band gap energy, it is apparent that the conductivity increases by almost 3 orders of magnitude. These preliminary findings highlight the feasibility of hypothesis (iii). On this basis, one could envision synthesizing a Se-rich surface on CZTS nanocrystals (i.e., formation of a CZTS/CZTSe core/shell material), thereby achieving high-efficiency PV devices through controlled surface chemistry without the need for a postdeposition annealing step.

We have shown that MCNs of $Cu_2ZnSn(S_{1-x}Se_x)_4$ can be successfully synthesized by the hot-injection method through careful tuning of the S and Se precursor reactivities. The composition dependence of the lattice parameters followed Vegard's law. Varying the value of $x$ from 0 to 1 resulted in a tunable band gap of 1.54 to 1.47 eV for $x = 0$ and 1, respectively. The synthesis of pure $Cu_2ZnSn(S_{1-x}Se_x)_4$ nanocrystals reported herein now provides an avenue for probing the effect of Se inclusion in mixed-chalcogenide thin films and may lead to new routes for the fabrication of highly efficient CZTS,Se nanocrystal PV devices without the need for postdeposition annealing.

## ■ ASSOCIATED CONTENT

**Supporting Information.** Details of nanocrystal synthesis and characterization, additional XRD analysis, low-magnification TEM images, UV−vis spectra, and conductivity data. This material is available free of charge via the Internet at http://pubs.acs.org.

## ■ AUTHOR INFORMATION

### Corresponding Author

bparkin1@uwyo.edu; Amy.Prieto@colostate.edu

### Current Address

[†]Materials Science Division and Argonne−Northwestern Solar Energy Research (ANSER) Center, Argonne National Laboratory, Argonne, Illinois 60439, United States.

## ■ ACKNOWLEDGMENT

We thank Dr. Gary Zito and Dr. John Chandler at the Colorado School of Mines for their assistance with HRTEM. Additional TEM imaging was supported in part by the Microscope Imaging Network core infrastructure grant from Colorado State University. This study was funded by the Center for Revolutionary Solar Photoconversion (CRSP).

## ■ REFERENCES

(1) Chen, L.-J.; Liao, J.-D.; Chuang, Y.-J.; Fu, Y.-S. *J. Am. Chem. Soc.* **2011**, *133*, 3704.
(2) Guo, Q.; Ford, G. M.; Hillhouse, H. W.; Agrawal, R. *Nano Lett.* **2009**, *9*, 3060.
(3) Guo, Q.; Ford, G. M.; Yang, W.-C.; Walker, B. C.; Stach, E. A.; Hillhouse, H. W.; Agrawal, R. *J. Am. Chem. Soc.* **2010**, *132*, 17384.
(4) Panthani, M. G.; Akhavan, V.; Goodfellow, B.; Schmidtke, J. P.; Dunn, L.; Dodabalapur, A.; Barbara, P. F.; Korgel, B. A. *J. Am. Chem. Soc.* **2008**, *130*, 16770.
(5) Shavel, A.; Arbiol, J.; Cabot, A. *J. Am. Chem. Soc.* **2010**, *132*, 4514.
(6) Steinhagen, C.; Panthani, M. G.; Akhavan, V.; Goodfellow, B.; Koo, B.; Korgel, B. A. *J. Am. Chem. Soc.* **2009**, *131*, 12554.
(7) Talapin, D. V.; Lee, J.-S.; Kovalenko, M. V.; Shevchenko, E. V. *Chem. Rev.* **2010**, *110*, 389.
(8) Chen, S.; Walsh, A.; Yang, J.-H.; Gong, X. G.; Sun, L.; Yang, P.-X.; Chu, J.-H.; Wei, S.-H. *Phys. Rev. B* **2011**, *83*, No. 125201.
(9) Chiang, M.-Y.; Chang, S.-H.; Chen, C.-Y.; Yuan, F.-W.; Tuan, H.-Y. *J. Phys. Chem. C* **2011**, *115*, 1592.
(10) Smith, D. K.; Luther, J. M.; Semonin, O. E.; Nozik, A. J.; Beard, M. C. *ACS Nano* **2011**, *5*, 183.
(11) Regulacio, M. D.; Han, M.-Y. *Acc. Chem. Res.* **2010**, *43*, 621.
(12) Riha, S. C.; Fredrick, S. J.; Sambur, J. B.; Liu, Y.; Prieto, A. L.; Parkinson, B. A. *ACS Appl. Mater. Interfaces* **2011**, *3*, 58.
(13) Riha, S. C.; Parkinson, B. A.; Prieto, A. L. *J. Am. Chem. Soc.* **2009**, *131*, 12054.
(14) Persson, C. *J. Appl. Phys.* **2010**, *107*, No. 053710.
(15) Schorr, S.; Gonzalez-Aviles, G. *Phys. Status Solidi A* **2009**, *206*, 1054.
(16) Todorov, T. K.; Reuter, K. B.; Mitzi, D. B. *Adv. Mater.* **2010**, *22*, E156.
(17) Katagiri, H.; Jimbo, K.; Yamada, S.; Kamimura, T.; Maw, W. S.; Fukano, T.; Ito, T.; Motohiro, T. *Appl. Phys. Express* **2008**, *1*, No. 041201.
(18) Guo, Q.; Hillhouse, H. W.; Agrawal, R. *J. Am. Chem. Soc.* **2009**, *131*, 11672.
(19) Wei, Y.; Yang, J.; Lin, A. W. H.; Ying, J. Y. *Chem. Mater.* **2010**, *22*, 5672.